



ELSEVIER

Journal of Structural Geology 25 (2003) 2023–2034

**JOURNAL OF
STRUCTURAL
GEOLOGY**

www.elsevier.com/locate/jsg

Can flat-ramp-flat fault geometry be inferred from fold shape?: A comparison of kinematic and mechanical folds

Heather M. Savage*, Michele L. Cooke

Morrill Science Center, University of Massachusetts Amherst, 611 North Pleasant St., Amherst, MA 01003, USA

Received 15 July 2002; received in revised form 7 November 2002; accepted 10 April 2003

Abstract

The inference of fault geometry from suprajacent fold shape relies on consistent and verified forward models of fault-cored folds, e.g. suites of models with differing fault boundary conditions demonstrate the range of possible folding. Results of kinematic (fault-parallel flow) and mechanical (boundary element method) models are compared to ascertain differences in the way the two methods simulate flexure associated with slip along flat-ramp-flat geometry. These differences are assessed by systematically altering fault parameters in each model and observing subsequent changes in the suprajacent fold shapes. Differences between the kinematic and mechanical fault-fold relationships highlight the differences between the methods. Additionally, a laboratory fold is simulated to determine which method might best predict fault parameters from fold shape. Although kinematic folds do not fully capture the three-dimensional nature of geologic folds, mechanical models have non-unique fold-fault relationships. Predicting fault geometry from fold shape is best accomplished by a combination of the two methods.

© 2003 Elsevier Ltd. All rights reserved.

Keywords: Fault-bend folding; Mechanical models; Kinematic models; Fault geometry prediction

1. Introduction

Constraining unexposed or poorly resolved subsurface fault geometry from observed fold shape has far-reaching importance, from assessment of seismic hazard to evaluation of hydrocarbon potential. Fault-bend folds have long been recognized as forming due to slip along subjacent faults with flat-ramp-flat geometry in areas of thin-skinned deformation (e.g. Rich, 1934; Mitra and Sussman, 1997) and past studies have shown that fault geometry has a systematic influence on aspects of fold shape such as axial trace orientation (Rowan and Linares, 2000), fold tightness (Allmendinger and Shaw, 2000) and fold terminations (Wilkerson et al., 2002). Within extensional environments fault depth and dip may be determined from the associated roll-over anticline, as long as the hanging wall stratigraphy is accurately determined (Williams and Vann, 1987; Kerr and White, 1992, 1994).

Both kinematic and mechanical models have been used to analyze fault-cored folds. Kinematic models, which balance the geometry of the deforming system without incorporating force or rheology, have been used extensively to study fault-bend folding (e.g. Suppe, 1983; Wilkerson et al., 1991; Salvini and Storti, 2001). Mechanical models utilize continuum mechanics to simulate deformation and have been used in the past to examine folding associated with fault ramp tips (e.g. Cooke and Pollard, 1997; Johnson and Johnson, 2001) and flat-ramp-flat geometry (e.g. Berger and Johnson, 1980; Kilsdonk and Fletcher, 1989; Strayer and Hudleston, 1997). A recent comparison of mechanical and kinematic trishear models of fault-tip folds (Johnson and Johnson, 2001) demonstrates the insights gained from comparative studies and exposes the dearth of such studies for fault-bend-folding. Within this study, two numerical models, one kinematic (fault parallel flow) and one mechanical (boundary element method), show how folds respond to changes in flat-ramp-flat fault geometry using these different methods. We perform a sensitivity analysis to ascertain which fault parameters are most influential over fold shape in each method. When kinematic and mechanical models with identical fault configurations produce similar

* Corresponding author. Present address, Department of Geosciences, The Pennsylvania State University, University Park, PA 16802, USA. Tel.: +1-413-545-2286; fax: +1-413-545-1200.

E-mail address: hsavage@geosc.psu.edu (H.M. Savage).

changes to a feature of the fold shape, the usefulness of that fold feature for inferring fault geometry is suggested. When the methods disagree, an attempt is made to determine if one set of generated fold shapes is more reasonable through comparison with field or laboratory models. Similar sensitivity analyses have focused on the effects of fault geometry (dip, ramp height, flat length, displacement) on fold shape in kinematic models (Rowan and Linares, 2000) and in mechanical models, along with the role of anisotropy, for fault propagation folds (Johnson and Johnson, 2001).

Finally, we perform kinematic and mechanical simulations of a laboratory fold with well-constrained fault geometry (Chester et al., 1991) in order to assess how accurately the models can predict a known fault geometry by matching the fold shape. The laboratory fold is simulated by iteratively altering fault geometry. The kinematic and mechanical best-fitting fault geometries are compared with the laboratory fault. Positive correlation of both fold and fault shapes supports use of the method for predicting subsurface fault geometry.

2. Modeling methods

2.1. Mechanical modeling

Mechanical modeling is based upon the three principles of continuum mechanics (e.g. Fung, 1969; Means, 1976; Timoshenko and Goodier, 1934). The first involves constitutive relationships, which relate the applied stress to the resulting strain in the rock (e.g. Means, 1976). The second principle of continuum mechanics states that the rock body must be in equilibrium; the body deforms but cannot translate or rotate (e.g. Means, 1976). The third principle, compatibility, requires that the displacement in each direction be continuous and single-valued to prevent gaps and overlaps from occurring (e.g. Means, 1976).

For this analysis we use POLY3D, a three-dimensional boundary element method (BEM) tool well suited for modeling faults (e.g. Crider and Pollard, 1998). BEMs discretize fault surfaces into a mesh of polygonal planar elements (Comninou and Dundurs, 1975; Thomas, 1994). POLY3D has been used to model normal fault interaction (Willems et al., 1996; Crider and Pollard, 1998; Maerten et al., 1999), as well as to assess the effect of segmentation on normal fault slip (Kattenhorn and Pollard, 2001). The user designates either slip/opening or traction on each element as well as a remote stress or strain. POLY3D assumes that the rock surrounding a fault is homogenous, isotropic and linear-elastic. Within our model, the rock body deforms in response to slip along faults in a half-space representing the upper Earth's crust (Fig. 1). Due to linear-elastic rheology, POLY3D evaluates stress most accurately under infinitesimal strain conditions (strain < 1%). However, the compatibility rules assure that displacements are single-valued even to large strains as long as the problem is

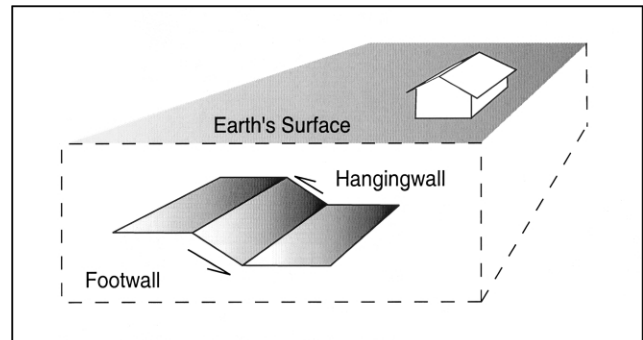


Fig. 1. Schematic diagram of POLY3D model. For this study, we set up a displacement boundary value problem by prescribing a remote strain of zero and slip amount to each element along the fault. The elastic half-space simulates the Earth's free surface.

set up as a displacement boundary value problem (Maerten, 1999; Maerten et al., 2000, 2001). In a displacement boundary value problem, the slip and opening are prescribed along fault elements rather than calculated from prescribed fault tractions and remote stress or strain. Furthermore, displacement boundary value problems require prescription of remote strains rather than stresses. To model large amplitude folds (i.e. > 1% strain) including simulation of laboratory folds, this study implements a displacement boundary value problem.

2.2. Kinematic modeling

Kinematic models use geometric constraints to analyze the progression of rock deformation. Such models are particularly beneficial for the geometric interpretation of faulted and folded terrains (e.g. Suppe, 1983; Williams and Vann, 1987; Geiser et al., 1988; Kerr and White, 1992). A variety of geometric rules can be applied to constrain the kinematics fault-cored folds including conservation of volume (e.g. Dahlstrom, 1990), fault parallel flow (Sanderson, 1982; Keetley and Hill, 2000), bed-parallel shear (e.g. Suppe, 1983) and inclined shear (Withjack and Peterson, 1993). Although flexural-slip based kinematic models are widely used to interpret deformation of sedimentary strata in contractional regimes (e.g. Suppe, 1983; Geiser et al., 1988), these algorithms are problematic for inferring fault geometry from fold shape without a priori knowledge of either fault shape or the axial surfaces of the fold. For this reason, the 3DMOVE kinematic analysis software (Midland Valley Ltd) implements fault-parallel flow (Kane et al., 2003) for reverse modeling and restorations of contractional folds. As suggested by the name, all points in the hanging wall displace parallel to the fault surface (Fig. 2). Bed area is conserved and, unless additional back-shear is applied to the hanging wall, beds thin along the forelimb of the fold. The computational robustness of the fault-parallel flow algorithm allows implementation of any fault shape in three-dimensions whereas bed-parallel slip algorithms are currently limited to two-dimensions. For our study, the

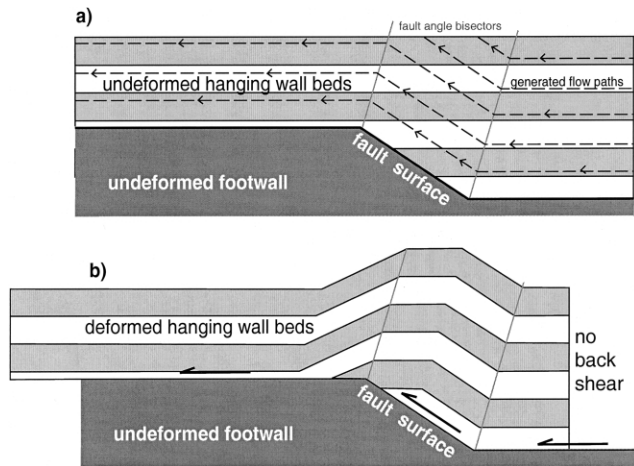


Fig. 2. Schematic diagram of the fault-parallel flow algorithm without added layer-parallel shear strain (Kane et al., 2003). (a) Each point within the hanging wall displaces along the generate flow lines (dashed) that parallel the fault surface within each dip domain. Dip domains are bounded by the bisectors to the fault kinks. (b) Without the application of additional layer-parallel shear, movement of the hanging wall is uniform within each dip domain resulting in a lengthened and thinned forelimb. This algorithm constrains the backlimb to parallel the ramp and fold amplitude equals throw on the fault. Because the same geometric rules apply to all beds, the fold shape is similar at all depths.

hanging wall moves up dip; however, the direction of transport can be oblique to fault dip (Fig. 2). As with mechanical methods, uniform or varied slip can be prescribed to fault surfaces. Unlike the mechanical methods, fault parallel flow and many other kinematic methods limit deformation to the hanging wall; the footwall remains fixed and undeformed.

3. Comparison of kinematic and mechanical methods

The analyses in this study outline the differences and similarities between mechanical and kinematic models of fault-bend folding. Fault parameters, including fault dip, depth, ramp length and amount of slip are systematically varied to assess their influence on anticline tightness, amplitude, length and width (Fig. 3). The three-dimensional fault surface consists of one rectangular ramp and lower and upper horizontal flat segments (Fig. 3). Within the fault parallel flow model, flats are considered to extend semi-indefinitely. Within the BEM models, the flats extend 15 km so that their distal tips do not influence folding over the ramp ($1 < \text{ramp length} < 10 \text{ km}$). Although flat depth is adjusted with variations in ramp length and depth, all other parameters of fault flats are constant. The flats and ramp extend 10 km in the strike directions in all models. Uniform reverse fault slip is prescribed directly to all fault segments. The ramp dips are varied to investigate a range of plausible fault geometries, which include those that may not have formed in contraction ($\text{dip} > 35^\circ$).

The fault parallel flow and boundary element methods

produce dramatically different shaped three-dimensional folds (Fig. 4). The kinematic anticline is boxy with a more steeply dipping backlimb than forelimb. The mechanical anticline is more domal than the kinematic fold and has an adjacent syncline. Deformation is more distributed in the mechanical fold as well, causing fold length to greatly exceed the length of the fault. For fault parallel flow models, fold length almost exactly corresponds to fault length.

For both fault parallel flow and BEM models the fold profiles along a dip-direction cross-section change with variation in fault geometry (Fig. 5). The model results are also graphed to detect trends in the fault-fold relations and highlight the differences between the kinematic and mechanical methods (Fig. A1). Understanding the relations between fault and fold parameters will facilitate inference of fault geometry from fold shape. For example, this will reduce the trial and error involved in estimating fault geometry from laboratory fold shape later in this paper.

3.1. Fold parameters

3.1.1. Fold tightness

The geometric nature of the kinematic method gives rise to a fold with a horizontal roof, with two sharp fold hinges where the roof and limbs meet (Fig. 4). Consequently, these folds have two interlimb angles to contribute to fold tightness (or openness), whereas the mechanical fold has a more rounded top and a single fold hinge. To facilitate comparison, fold tightness is here expressed in terms of difference between limb dips rather than interlimb angle.

All of the kinematic folds have more steeply dipping forelimbs and backlimbs than the mechanical folds; consequently, the kinematic folds generally have greater tightness (Fig. 5). Kinematic fold tightness positively correlates with fault dip (Fig. 5d); steeper ramps produce tighter folds.

The mechanical fold tightness is affected by all of the fault ramp parameters. Increase in ramp length slightly tightens folds (Figs. 5e and A1b). However, once the ramp length exceeds 5 km, further increases in ramp length have little effect on fold tightness (Fig. 5e). Similarly, increasing depth of the fault broadens the fold until the fault reaches 2–3 km depth, when the rate of change drops considerably (Fig. 5g). Mechanical fold tightness is most sensitive to fault depth, followed by fault slip. In this analysis of fold tightness, two differences between the BEM and fault parallel flow models emerge; while mechanical folds become tighter with increased fault slip and shallower fault depth, the kinematic fold tightness remains unchanged. Because tighter folds associated with increased slip are observed in laboratory experiments (Chester et al., 1991), we consider the mechanical method to more reliably incorporate this relationship than the kinematic method.

Increasing fault dip tightens folds in both fault parallel flow and BEM models (Fig. 5c and d) as well as other kinematic models (Rowan and Linares, 2000). However, the

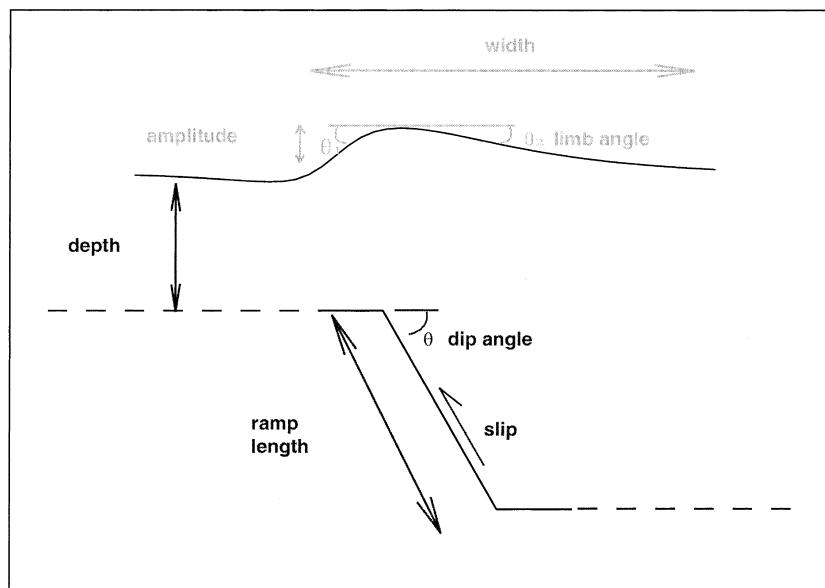


Fig. 3. Fault parameters (in dark gray) are varied to assess their effects on fold parameters (in light gray). Fold length (in and out of the page) is measured as well.

forelimb and backlimb dips of the kinematic fold are constrained by ramp dip (Fig. 2; Kane et al., 2003), whereas the dips of both limbs change in the BEM model with slip amount and depth. The insensitivity of kinematic fold tightness to fault depth contradicts field observations of fault-bend folds where layers become more open away from the fault ramp (Rowan and Linares, 2000). Such tightening of folds near ramp tips has been frequently observed in fault-tip folds (e.g. Davis, 1978; Chester et al., 1988). However, using fold tightness to infer fault parameters based on the BEM model results are problematic and non-unique because all of the fault parameters have significant effects on fold tightness.

3.1.2. Fold amplitude

Fold amplitude is measured vertically between the crest of the fold and the surface far away from the fold. Fault slip magnitude has the greatest effect on fold amplitude in both fault parallel flow and BEM models; slip is directly proportional to amplitude (Figs. 5a and b and A1e). In the kinematic fold, this relationship results from the increased throw associated with increased slip vector. For instance, 2 km of slip along a 45° dipping fault produces 1.4 km of throw whereas 1 km of slip produces half as much throw. Consequently, steeper ramps also produce greater amplitude folds because they have greater throw, the upward component of slip (Fig. 5d). For the fault parallel flow

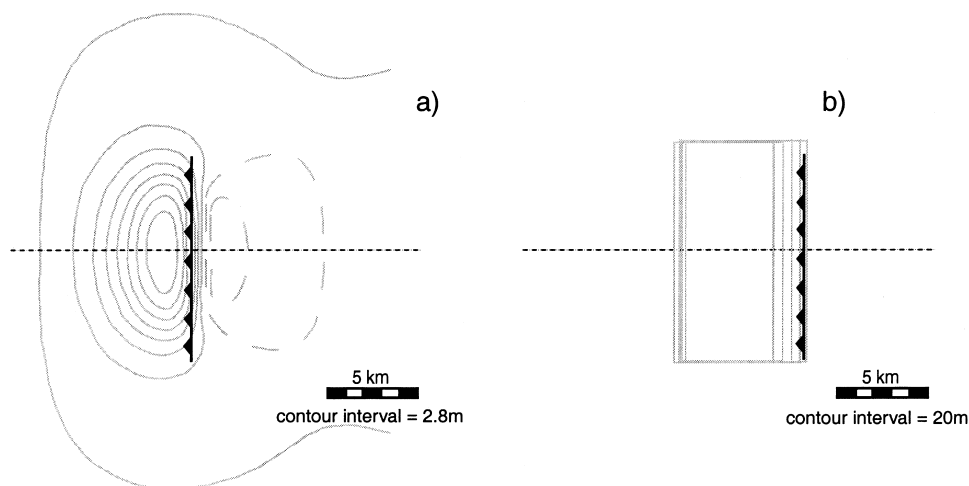


Fig. 4. Map view of (a) mechanical (BEM) and (b) kinematic (fault parallel flow) fold contours resulting from 1 km of slip along a 10 km ramp buried 2 km. The dashed contours of the mechanical fold signify an amplitude of less than zero corresponding to syncline development. Dotted line indicates transect used for fold profile analysis (Fig. 5).

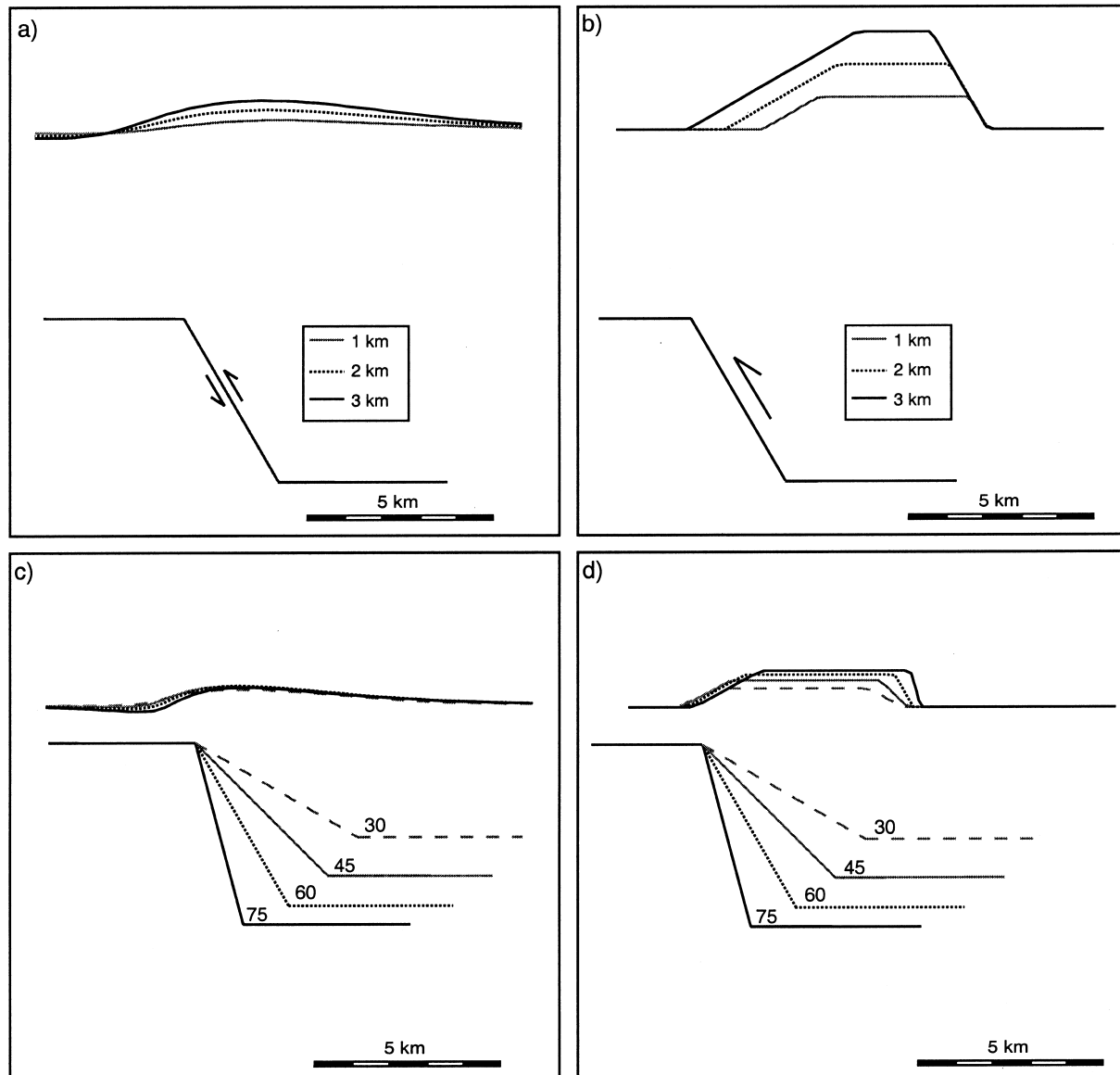


Fig. 5. Change in fold profiles for mechanical (left column) and kinematic (right column) folds. While one fault parameter is varied, all other parameters are held constant. When slip is changing (row 1), the depth is held at 5 km, the ramp length at 5 km, the fault dip at 60° . While varying the dip of the fault (row 2), slip is held constant at 1 km, the ramp length at 5 km and the depth at 1 km. During variation in ramp length (row 3), the slip is held at 1 km, the dip at 60° and the depth at 1 km. Finally, while depth of the fault is varied (row 4), the slip is held at 1 km, the ramp length at 5 km and the dip at 60° .

models these parameters are directly related by geometry; fold amplitude is equal to the sine of the fault dip multiplied by the prescribed slip. Because the sine function varies between zero and one, while the amount of slip can exceed one, variation in fault slip more strongly affects amplitude than fault dip (Fig. 5b and d). An increase in fold amplitude with increased slip also occurs in laboratory models of folding (Morse, 1977; Chester et al., 1991).

The mechanical fold amplitude is influenced by all fault parameters, although most significantly by slip amount. Mechanical fold amplitude is positively correlated with fault slip, dip and length while deeper fault ramps produces slightly smaller fold amplitudes (Fig. 5a, c, e and g). Whereas deeper ramps produce smaller surface folds, longer

and steeper fault ramps produce greater amplitude folds. Although amplitude is positively correlated with slip for both models, the kinematic fold amplitude is more sensitive to slip amount than the mechanical fold. Because BEM models experience displacement along both sides of the fault, i.e. the hanging wall displaces up-dip as the footwall displaces down-dip, the hanging wall experiences approximately one half the slip movement in contrast to the fault parallel flow models, which only have displacement on the hanging wall side of the fault ramp. Therefore, the hanging wall of the BEM model experiences half the deformation of the kinematic hanging wall for the same amount of slip. The remaining deformation is accommodated within the footwall of the mechanical models.

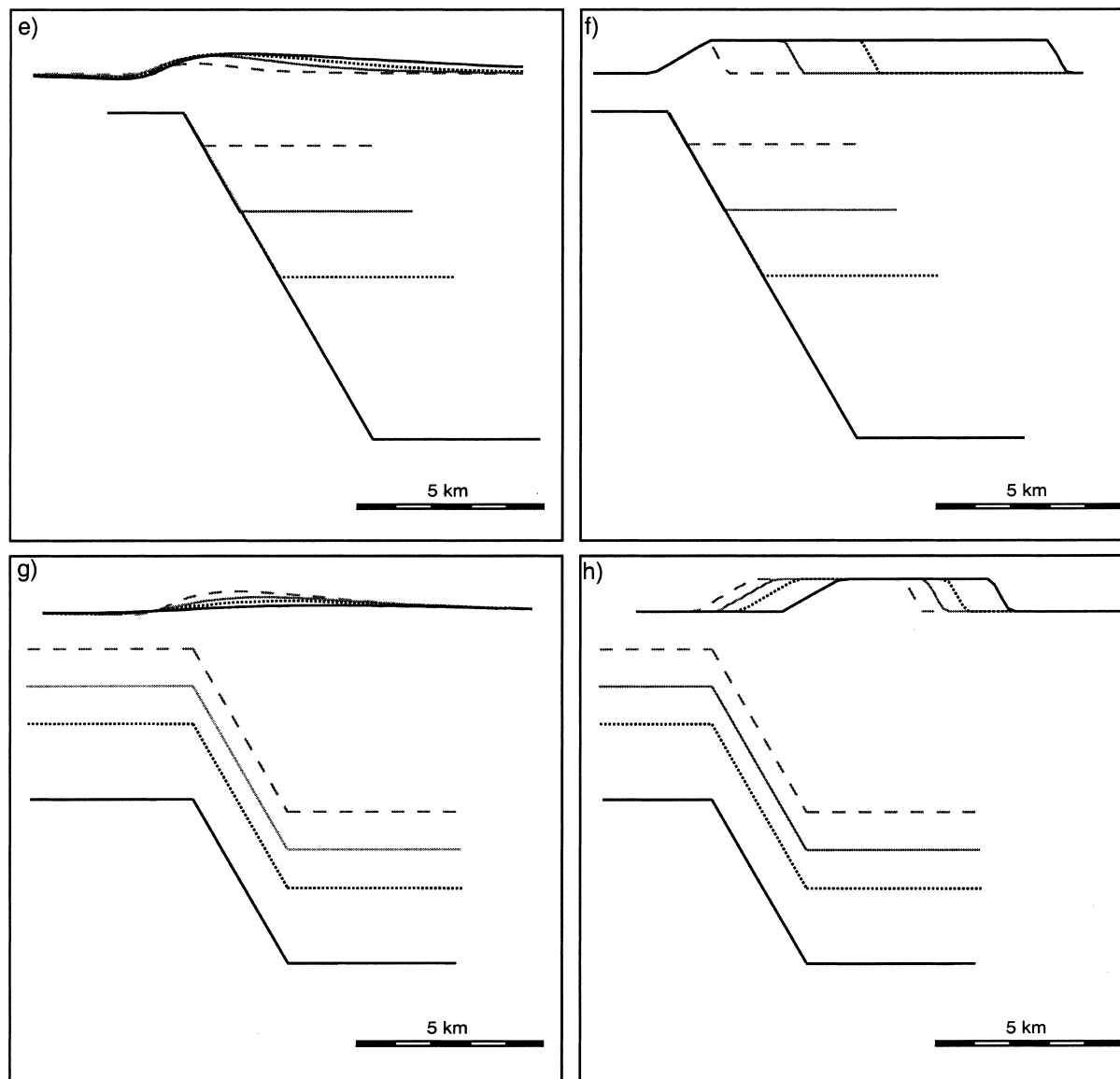


Fig. 5 (continued)

The kinematic method may overestimate fold amplitude because amplitude depends only on the slip and dip of the fault and is independent of fault depth for these models. As mentioned earlier, we expect layers further away from a fault tip to have less deformation but the fault parallel flow models predict no such decrease. Therefore when using fold amplitude to infer fault slip, the kinematic result cannot be used unless the ramp depth is known.

The fold shape also responds to changes in fault dip (Fig. 5c and d; Rowan and Linares, 2000). Folds overlying steeper faults have greater amplitude in both fault parallel flow and BEM models due to the greater component of vertical displacement along these faults. However, for fault dip greater than 60° , the mechanical fold amplitude decreases (Fig. 5c). Because the BEM models incorporate

displacement along both sides of the fault, downward displacement of the footwall creates a small syncline ahead of the forelimb (Fig. 5a, c, e and g). When the depth of the syncline is added to the height of the anticline, this aggregate fold amplitude has a similar correlation with fault ramp dip as the kinematic fold (see Fig. A1). This approach was not used as the standard to measure fold amplitude because the fault parallel flow models do not produce a syncline and the direct comparison would be compromised. While ramp dip affects fold amplitude, the fold tightness and width are more accurate constraints on this fault parameter.

Ramp length increases fold amplitude very slightly for both sets of models (Fig. 5g and h). The increase in fold amplitude becomes less discernible with increasing ramp length. This indicates that miscalculating an 8-km ramp as a

10-km ramp will not affect the results as much as miscalculating a 1-km ramp as a 3-km ramp.

3.1.3. Fold length

Slightly different methods of fold length measurement are used for fault parallel flow and BEM models because of the difference in fold termination style. Mechanical folds do not terminate as abruptly as kinematic folds (Fig. 4). For the fault parallel flow models, the fold length extends to the locations where fold amplitude along the fold height abruptly drops to zero. The mechanical fold terminations are estimated where the amplitude along the fold axis drops to 1% of the maximum amplitude, because the surface is not exactly zero after folding. One of the most significant distinctions between the models is the influence of fault length on suprajacent folding. The kinematic fold length depends solely on the length of the fault at a nearly one-to-one ratio; no other fault parameter affects fold length. Because the fault parallel flow method is created by linking two-dimensional cross-sections, material only moves within the user-prescribed transport plane. Consequently, the fold takes on a boxy shape, with the nose of the fold falling off abruptly above the lateral end of the fault (Fig. 4b). In contrast, the mechanical fold length ranges from two to five times the length of the fault. The mechanical fold lengths correlate positively with fault dip, depth and slightly with ramp length because in continuum mechanics, deformation at one point influences the surrounding material. To distinguish between the kinematic and mechanical predictions for fault length, high quality three-dimensional seismic or laboratory data would be needed to ascertain how far natural folds extend beyond fault terminations; the authors are unaware of such published data. However, when the length of the fault is not a major consideration, such as studies of cylindrical folds, this inherent difference in the models may not be important.

3.1.4. Fold width

Fold width is measured in the same manner as fold length, where the fold amplitude drops to zero or 1% of the maximum fold amplitude for the fault parallel flow and BEM models, respectively. An increase in the fault ramp length creates wider folds for both models of this (Fig. 5g and h) and other studies (Rowan and Linares, 2000). Fold width is most sensitive to ramp length and this is the only significant effect that ramp length has on kinematic fold geometry (Fig. 5). Fold width increases with increasing ramp length similarly for both models, except the BEM models are consistently 7 km wider, due to the more distributed nature of deformation in these models. Whereas deformation in the fault parallel flow models is limited to the hanging wall above and ahead of the ramp, in the BEM models, material below and behind the ramp also deforms. The laboratory study by Chester et al. (1991) shows that folds are wider than the length of the ramp, indicating that

the mechanical folds are more consistent with laboratory folding.

Although fold width is most sensitive to ramp length in both sets of models, other parameters also affect fold width. While kinematic fold width is insensitive to fault dip, mechanical folds become narrower with increasing fault dip (Fig. 5c and d). Additionally, fold width is positively correlated with fault slip; however, kinematic fold width increases more dramatically with slip than mechanical folds (Fig. 5a and b). Laboratory fault-bend fold models that test different ramp dips are not prevalent in the literature. However, laboratory models that vary fault slip show that fold width increases with increased in fault slip (Chester et al., 1991).

3.2. Significant difference between kinematic and mechanical methods

The over-arching difference between the kinematic and mechanical methods is not a difference in resultant fold shapes but rather a difference in the way each method simulates deformation. In the kinematic method, each fold parameter is sensitive to only one or two fault ramp parameters (Table 1). In contrast, the BEM model results are more nuanced; fold aspects are sensitive to several fault ramp parameters. This leads to ambiguity and non-uniqueness when inferring fault geometry from fold shape using the mechanical results. An example of this is shown in Fig. 6 where similar fold shapes are formed from faults with different dips, depths, and horizontal placement of the ramp tip. Therefore, when using fold shape to infer fault shape, the kinematic method should be used to produce a non-unique first approximation, but will be unreliable for final results due to lack of out-of-transport plane movement and uniform fold shape with fault depth.

4. Comparison to laboratory fault-bend fold models

By simulating a laboratory experiment with well-constrained fold and fault shapes we can test how closely the kinematic and mechanical models predict the fault

Table 1
Sensitivity of fold aspects to fault ramp parameters. K—kinematic: fault slip affects fold amplitude and width, ramp dip affects fold tightness, ramp length affects fold width, and ramp length affects fold length. M—mechanical: all fold parameters are affected by at least two fault ramp parameters

	Slip	Ramp length	Dip	Depth
Fold amplitude	M, K		M	M
Fold length		M	M	M
Fold width	M, K	M, K	M	
Fold tightness	M	M	M, K	M

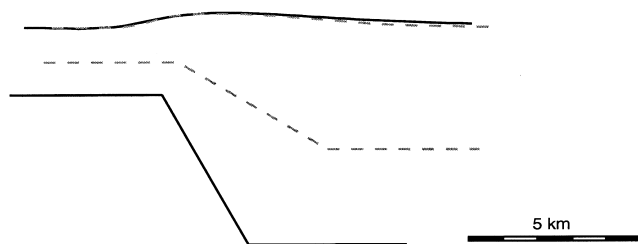


Fig. 6. Two faults with different depths and dips produce remarkably similar fold shapes using the mechanical method. The black fault dips 60° and is 2 km below the surface while the gray fault dips 20° and is 1 km below the surface.

geometry from the fold shape. Because of the lack of out-of-transport plane movement in the kinematic method, we chose a non-plunging fold experiment, where stretching in the third dimension is not a factor.

Chester et al. (1991) produced fault-bend folds by compressing rock layers situated over a fault in a triaxial compressor (Fig. 7a). The folded layers were limestone interbedded with either mica or lead to promote interlayer slip. During interlayer slip, weak contacts in a stack of layered rock act as fault surfaces as the rock is folded, allowing greater bending than a homogenous body of the same thickness and creating a higher, tighter fold (Pollard and Johnson, 1973). Experimental interlayer slip along mica or lead layers simulates geologic slip along layers with low

shear strength such as shale. A forcing block of sandstone with a pre-existing, lubricated fault surface was used to fold the limestone and mica layers. A rigid block of either granite or sandstone composed the footwall of the fault to simulate thin-skinned deformation. The fault ramp is approximately 0.57 cm deep, dipping 20° , 1.53 cm long and, in the particular experiment simulated here (Chester et al., 1991; Fig. 7a), the fault has approximately 0.71 cm of slip. The resultant fold is 0.32 cm in amplitude, 3.9 cm wide, with a forelimb angle of about 17° and a 17° dipping backlimb (Fig. 7a).

A series of fault parallel flow and BEM models were iteratively altered until the model fold shapes approximated the laboratory fold shape (Fig. 7a). The fault geometry of the laboratory experiment served as the initial model configuration in this iterative process. Once a match is made to the fold shape, the model faults are compared with the laboratory fault geometry to determine which method could more accurately determine fault geometry from fold shape. Although the mechanical models could yield multiple fault configurations that produce fold shapes matching the laboratory fold, we limit the chance of spurious matches by using the laboratory geometry as the initial model configuration. In the absence of data to constrain a hypothetical initial geometry, the iterative matching of fold shape can become time consuming and,

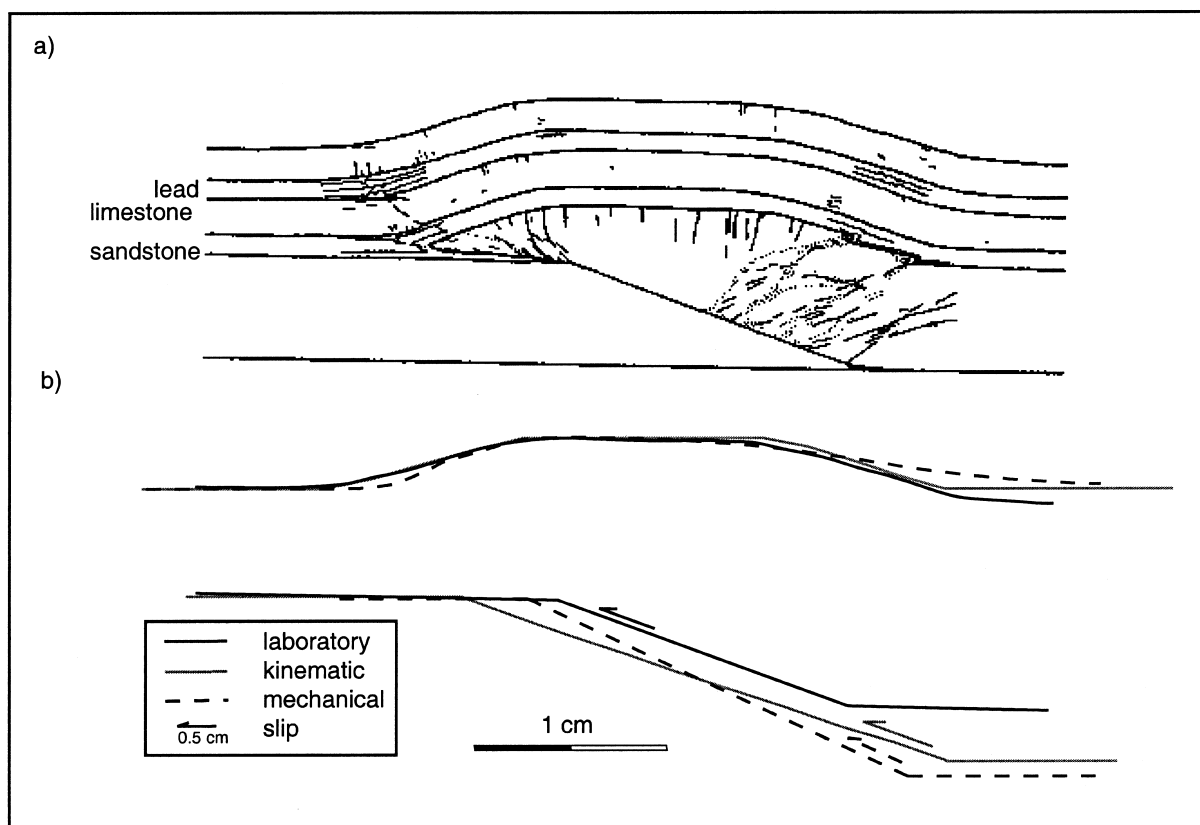


Fig. 7. (a) Laboratory fault-bend fold (Chester et al., 1991). (b) Fold profiles produced by laboratory fold (black), kinematic fold (gray) and mechanical fold (dashed black). The fault parallel flow model more closely approximates the fold shape than the BEM.

when using mechanical methods, can yield inaccurate fault configurations.

Slip along the laboratory fold exceeds 50% of the ramp length. Simulating such high ratios of slip to ramp length can be problematic for mechanical models that assume linear elasticity. To avoid this the mechanical models that simulate Chester's laboratory folding, are incremented so that the slip in any one step is much less than ramp length.

When simulating the laboratory fold, fault depth is the most difficult of the fault parameters to infer. The kinematic method is insensitive to fault depth, as fault depth only alters lateral position of the suprajacent fold (Fig. 5h), and the mechanical method calculates flexure of a homogenous block which predicts shallower faults than an equivalent method incorporating interlayer slip. However, interlayer slip can be simulated within the BEM models by determining the effective thickness of a homogenous block with the same resistance to bending as a freely-slipping layered sequence; this effective thickness is usually much smaller than the total thickness of the layered rock (Pollard and Johnson, 1973). For this laboratory experiment, the effective thickness of the layers is equivalent to the effective depth of the fault (Fig. 7a). The effective depth of the laboratory fault is calculated with the equation:

$$D_e = (Dt^2)^{1/3} \quad (1)$$

where D_e is effective fault depth, D is the actual fault depth and t is thickness of individual layers (Pollard and Johnson, 1973). This equation is only valid for free-slipping layers with approximately uniform elastic constants and thickness, such as those in the experiment of Chester et al. (1991). For this laboratory model, the effective depth of the upper ramp tip is 0.23 cm. We modeled a fault at this depth and iteratively altered other parameters until we arrived at the best-fitting fold shape. Interlayer slip can be incorporated within the BEM model by considering the effective depth of the fault but cannot be considered in the fault parallel flow model due to the insensitivity of this method's fold shape to fault depth.

From this analysis, the two methods predict surprisingly similar fault geometry from fold width and amplitude and the discrepancy between the predicted and laboratory fault geometries is similar for kinematic and mechanical models. The kinematic model infers the fault ramp approximately 0.5 cm ahead of the laboratory upper ramp tip, but kinematic fault depth also influences inference of fault position. With increasing kinematic fault depth, the suprajacent fold position shifts to the right, which subsequently shifts the inferred fault position (Fig. 5h). In this simulation, we constrained fault depth from the laboratory experiment. This suggests that either fault depth or lateral position will need to be constrained to infer geologic faults.

Assessment of the overall shapes of the folds (Fig. 7) reveals that the kinematic fold approximates the Chester

et al. (1991) fold slightly more accurately than the mechanical fold. The kinematic and laboratory folds are nearly symmetric while the forelimb of the mechanical fold is slightly steeper than the backlimb.

Both methods simulate the laboratory fold shape well and predict reasonable fault parameters. The kinematic model overpredicts slip in order to match fold amplitude, whereas the mechanical predicts slip accurately. Both methods overpredict ramp length in order to match fold width. This discrepancy could mean that the laboratory fold experiences deformation not incorporated in either of the models. For example, microcracking and associated dilation observed in the experiment (Chester et al., 1991) may produce more distributed deformation than that of the models, resulting in wider folding.

Another difference between the models and the laboratory test is the application of uniform slip along ramp and flats in both the mechanical and kinematic models. This assumption facilitates the inference of fault geometry by reducing the number of unknowns but does not accurately simulate the laboratory deformation. Within the laboratory and in natural folds, faulting and subsequent folding are driven by far-field (tectonic) contraction, which does not typically yield uniform slip. Variations in slip distribution are expected to produce variations in limb dip, fold width and other parameters. Furthermore, tectonic contraction may act to tighten folds produced by slip along underlying faults.

5. Discussion

Both the kinematic (fault parallel flow) and mechanical (BEM) models have similar levels of accuracy for inferring fault geometry from the shape of two-dimensional folds (Table 2). Either model could be used to infer the ramp geometry, but the mechanical model inferred slightly more accurate fault slip and is needed to constrain fault depth.

Table 2

Analysis of modeled fold and fault measurements compared with laboratory fold. *The mechanical fold width is taken at 5% of the maximum amplitude because of the difficulty of distinguishing where the laboratory fold fell to 1% maximum amplitude

	Laboratory	Mechanical	Kinematic
Fold parameters			
Amplitude (cm)	0.32	0.31	0.33
Width (cm)*	3.9	4.6	3.67
Forelimb (°)	17	25	16
Backlimb (°)	17	9	16
Fault parameters			
Slip (cm)	0.71	0.7	1.18
Dip (°)	20	25	16
Ramp length (cm)	1.46	2.2	2.2
Depth	0.57	0.57	Insensitive
Effective depth	0.23	0.23	–

However, in the unlikely scenario that the lateral position of fault ramp is known and depth is unknown, the kinematic method can constrain ramp depth. Both models overestimate the ramp length needed to simulate the laboratory fold. For constraining fault length along fold axis, further three-dimensional laboratory analysis is needed.

The one-to-one relationship of fault and fold parameters for the kinematic method lent ease inferring fault geometry from the Chester et al. (1991) laboratory fold. In contrast, the interactive nature of the fault and fold parameters in the mechanical model leads to non-uniqueness of fold shape, i.e. more than one fault geometry may produce the same fold shape. Because the fault shape of the Chester et al. (1991) experiment was our first guess, the iterative matching converged on a fault geometry similar to the laboratory fault. A drastically different first-guess fault could have resulted in iterative convergence on a very

different mechanical fault geometry that also matches the laboratory fold shape.

To resolve this non-uniqueness, more than one method can be used. When out-of-transport-plane deformation is not a significant factor, the fault parallel flow kinematic method would provide a good first approximation. However the suitability of this method decreases for plunging folds or in areas where multiple faults interact. In areas of significant three-dimensional deformation or in areas of multiple coeval faults, the kinematic model should not be taken as a final approximation. Furthermore, the limits of the kinematic method to constrain fault depth provides the need for an additional method in any circumstance.

A drawback to directly inferring fault geometry from the shape of folded sedimentary layers with the mechanical model is the lack of implicit interlayer slip. However, this

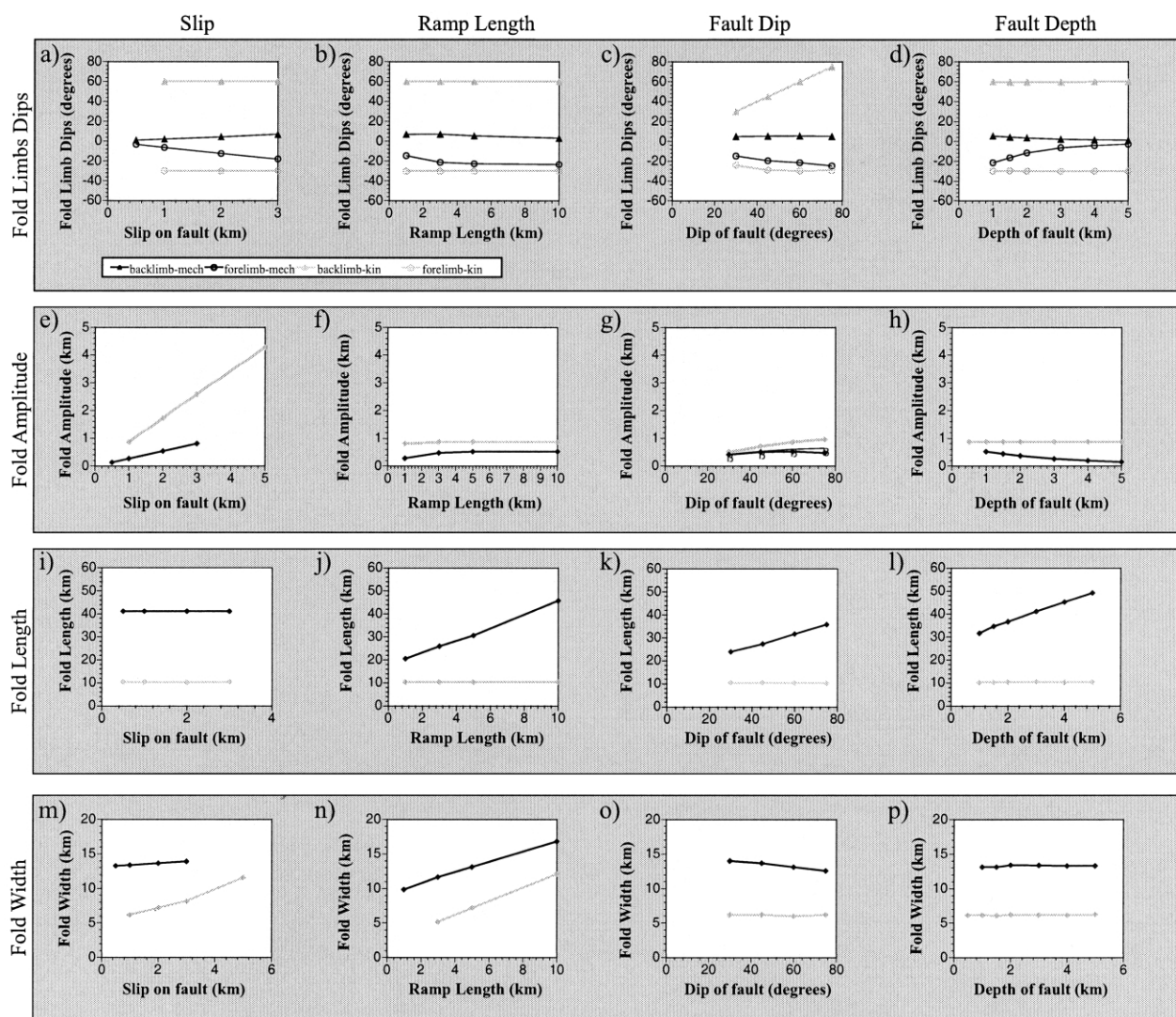


Fig. A1. Fold shape variation shown graphically (a–p). The kinematic models are shown in gray and the mechanical models in black. Fig. 4g shows a dark gray trend that signifies the effect of fault dip on fold amplitude when height of the fold and depth of the syncline are both considered.

can be remedied by implementing the effective thickness of the strata into the model.

6. Conclusions

Detailed comparison of kinematic and mechanical forward-modeled fold shapes highlight inherent differences between the two methods. Kinematic fold parameters generally respond to changes in one fault parameter while the interplay between mechanical fold and fault parameters renders non-unique inferences of fault geometry from fold shape. Consequently, a multi-proxy approach, incorporating field data and constraints from other types of models, is suggested. Both methods simulate fault/fold relationships relatively well and when used in conjunction, offer a powerful tool for predicting fault geometry from fold shape.

Acknowledgements

We thank Kaj Johnson and an anonymous reviewer for insightful comments that greatly improved this paper. We also thank Chris Okubo for reading a very early draft of this paper. Fault parallel flow analysis was performed with 3DMOVE software by Midland Valley Exploration, Ltd. Figure 1 was drafted by Tye Numelin.

Appendix A

Fig. A1

References

- Allmendinger, R., Shaw, J., 2000. Estimation of fault propagation distance from fold shape; implications for earthquake hazard assessment. *Geology* 28 (12), 1099–1102.
- Berger, P., Johnson, A.M., 1980. First-order analysis of deformation of a thrust sheet moving over a ramp. *Tectonophysics* 70, T9–T24.
- Chester, J.S., Logan, J.M., Spang, J.H., 1988. Comparison of thrust models to basement-cored folds in the Rocky Mountain foreland. In: Schmidt, C.J., Perry, W.J., Jr. (Eds.), *Interaction of the Rocky Mountain Foreland and the Cordilleran Thrust Belt*. Geological Society of America Memoir 171, pp. 65–74.
- Chester, J.S., Logan, J.M., Spang, J.H., 1991. Influence of layering and boundary conditions on fault-bend and fault-propagation folding. *Geological Society of America Bulletin* 103 (8), 1059–1072.
- Comninou, M., Dundurs, J., 1975. The angular dislocation in a half-space. *Journal of Elasticity* 5, 205–216.
- Cooke, M., Pollard, D.D., 1997. Bedding-plane slip in initial stages of fault-related folding. *Journal of Structural Geology* 19, 567–581.
- Crider, J.G., Pollard, D.D., 1998. Fault linkage: 3D mechanical interaction between echelon normal faults. *Journal of Geophysical Research* 103, 24373–24391.
- Dahlstrom, C.A., 1990. Geometric constraints derived from the law of conservation of volume and applied to evolutionary models for detachment folding. *AAPG Bulletin* 74 (3), 336–344.
- Davis, G.H., 1978. The monocline fold pattern of the Colorado Plateau. In: Matthews, V. (Ed.), *Laramide Folding Associated with Basement Block Faulting in the Western United States*. Geological Society of America Memoir 151, pp. 215–233.
- Fung, Y.C., 1969. *A First Course in Continuum Mechanics*, Prentice-Hall, Englewood Cliffs, NJ.
- Geiser, J., Geiser, P.A., Kligfield, R., Ratliff, R., Rowan, M., 1988. New applications of computer-based section construction: Strain analysis, local balancing and subsurface fault prediction. *The Mountain Geologists* 25(2), 47–59.
- Johnson, K., Johnson, A., 2001. Mechanical analysis of the geometry of forced-folds. *Journal of Structural Geology* 24, 401–410.
- Kane, S.J., Williams, G.D., Buddin, T.S., 2003. A generalised flow approach to section restoration—fault bend folding. In preparation.
- Kattenhorn, S.A., Pollard, D.D., 2001. Integrating 3-D seismic data, field analogs, and mechanical models in the analysis of segmented normal faults in the Wytch Farm oil field, southern England, United Kingdom. *American Association of Petroleum Geologists Bulletin* 85 (7), 1183–1210.
- Keetley, J.T., Hill, K.C., 2000. 3D structural modeling of the Kutubu oil fields, PNG. In: *AAPG International Conference and Exhibition; Abstracts 84*. American Association of Petroleum Geologists, 1446.
- Kerr, H.G., White, N., 1992. Laboratory testing of an automatic method for determining normal fault geometry at depth. *Journal of Structural Geology* 14, 873–885.
- Kerr, H.G., White, N., 1994. Application of an automatic method for determining normal fault geometries. *Journal of Structural Geology* 16, 1691–1709.
- Kilsdonk, B., Fletcher, R.C., 1989. An analytical model of hanging-wall and footwall deformation at ramps on normal and thrust faults. *Tectonophysics* 163, 153–168.
- Maerten, L., 1999. Mechanical interaction of intersecting normal faults: theory, field examples and applications. Ph.D. Thesis, Stanford University.
- Maerten, L., Willemsse, E.J.M., Pollard, D.D., Rawnsley, K., 1999. Slip distributions on intersecting normal faults. *Journal of Structural Geology* 21, 259–271.
- Maerten, L., Pollard, D.D., Karpuz, R., 2000. How to constrain 3-D fault continuity and linkage using reflection seismic data: a geomechanical approach. *American Association of Petroleum Geologists Bulletin* 84, 1311–1324.
- Maerten, L., Gillespie, P., Pollard, D.D., 2001. Effect of local stress perturbation on secondary fault development. *Journal of Structural Geology* 24, 145–153.
- Means, W.D., 1976. *Stress and Strain*, Springer-Verlag, New York.
- Mitra, G., Sussman, A.J., 1997. Structural evolution of connecting splay duplexes and their implications for critical taper: an example based on geometry and kinematics of the Canyon Range culmination, Sevier Belt, central Utah. *Journal of Structural Geology* 19 (3-4), 503–522.
- Morse, J., 1977. *Deformation in the Ramp Regions of Overthrust Faults; Experiments with Small-scale, Rock Models*, Wyoming Geological Association, Casper, WY.
- Pollard, D.D., Johnson, A.M., 1973. Mechanics of growth of some laccolithic intrusions in the Henry Mountains, Utah; II, Bending and failure of overburden layers and sill formation. *Tectonophysics* 18 (3-4), 311–354.
- Rich, J.L., 1934. Mechanics of low-angle overthrusting as illustrated by Cumberland thrust block, Virginia, Kentucky and Tennessee. *Bulletin of the American Association of Petroleum Geologists* 18 (12), 1584–1596.
- Rowan, M.G., Linares, R., 2000. Fold-evolution matrices and axial-surfaces of fault-bend folds; application to the Medina Anticline, Eastern Cordillera, Columbia. *AAPG Bulletin* 84 (6), 741–764.
- Salvini, F., Storti, F., 2001. The distribution of deformation in parallel fault-related folds with migrating axial surfaces: comparison between fault-propagation and fault-bend folding. *Journal of Structural Geology* 23, 25–32.

- Sanderson, D.J., 1982. Models of strain variation in nappes and thrust sheets; a review. *Tectonophysics* 88 (3-4), 201–233.
- Strayer, L.M., Hudleston, P.J., 1997. Numerical modeling of fold initiation at thrust ramps. *Journal of Structural Geology* 19 (3-4), 551–566.
- Suppe, J., 1983. Geometry and kinematics of fault-bend folding. *American Journal of Science* 283 (7), 684–721.
- Thomas, A.L., 1994. POLY3D: A Three-Dimensional, Polygonal Element, Displacement Discontinuity Boundary Element Computer Program with Applications to Fractures, Faults and Cavities in the Earth's Crust. Ph.D. thesis, Stanford University.
- Timoshenko, S.P., Goodier, J.N., 1934. *Theory of Elasticity*, McGraw-Hill Book Company, New York.
- Wilkerson, M.S., Medwedeff, D.A., Marshak, S., 1991. Geometrical modeling of fault-related folds: a pseudo-three-dimensional approach. *Journal of Structural Geology* 13, 801–812.
- Wilkerson, M.S., Apotria, T., Farid, T., 2002. Interpreting the geologic map expression of contractional fault-related fold terminations: lateral/oblique ramps versus displacement gradients. *Journal of Structural Geology* 24, 593–607.
- Willemsse, E.J.M., Pollard, D.D., Aydin, A., 1996. Three-dimensional analyses of slip distributions on normal fault arrays with consequences for fault scaling. *Journal of Structural Geology* 18 (2/3), 295–309.
- Williams, G., Vann, I., 1987. The geometry of listric normal faults and deformation in their hanging walls. *Journal of Structural Geology* 9, 789–795.
- Withjack, M.O., Peterson, E.T., 1993. Prediction of normal-fault geometries—a sensitivity analysis. *AAPG Bulletin* 77 (11), 1860–1873.